The Visual Computer

Visualization of optical phenomena caused by multilayer films based on wave optics

H. Hirayama[1], K. Kaneda[1], H. Yamashita[1], Y. Yamaji[1], Y. Monden[2]

[1] Faculty of Engineering, Hiroshima University, 1-4-1 Kagamiyama, Higashi-hiroshima, 739-8527, Japan
[2] Interdisciplinary Faculty of Science and Engineering, Shimane University, 1060 Nishikawatsu, Matsue, 690-8504, Japan
email: {hira,kin,yama,san}@eml.hiroshima-u.ac.jp
monden@cis.shimane-u.ac.jp

This paper proposes a method for rendering objects coated with multilayer thin films, taking into consideration multiple reflection and refraction, interference, and absorption of light inside the films. The proposed method is based on wave optics, and it can accurately visualize the optical effects of multilayer films consisting of not only dielectric materials, but also metallic and semiconductive materials. Optical properties of a SiO_2 film coating on a silicon base, and several kinds of multilayer films coating windowpanes, glasses, or teapots are visualized to demonstrate the usefulness of the proposed method.

Key words: Multilayer thin film – Multiple reflection and refraction – Interference – Complex refractive index – Composite reflectance and transmittance

Correspondence to: H. Hirayama

1 Introduction

Visual effects caused by multilayer thin films can be exquisite. Rainbow colors appear on a lens coated with multilayer thin films due to interference of light within the films. Multilayer thin films are also used in industry, for example, for optical lenses, optical filters, windowpanes, and surfaces of cars. They are designed to have good optical efficiency or a pleasant appearance. It is necessary to evaluate optical properties of multilayer films in the design process.

Traditionally, reflectance and transmittance of the films are displayed in graph format to evaluate their optical properties (Fig. 8). However, understanding the properties of the graphs has proved difficult, as the properties change considerably with both changing direction and wavelength of light. Added to this is the fact that much experience and knowledge are required to understand the graphs. For these reasons, it is desirable to visualize the optical effects of multilayer films with the technique of computer graphics, and many researchers have thus tried to render the optical phenomena generated by such thin films.

Research on realistic rendering of optical phenomena began in early 1980s. A method based on wave optics was developed to render the diffraction of light [14]. Methods for rendering metals [2] and transparent objects [9, 22] with the Fresnel formulae were also developed. Furthermore, the dispersion of light [21] was taken into account for rendering optical phenomena caused by transparent objects, such as a prism, and the scattering of light inside transparent objects [23] was taken into account for rendering chatoyancies of gems. Methods for rendering optical phenomena caused by thin films or layered objects have been developed since 1990. Thin film or various kinds of objects coated with films have been rendered, including soap bubbles [3, 13, 20], Newton's rings [4, 19], skin (scattering of light inside layers under the skin [10] was taken into account), optical effects of paints [8], metals coated with multilayer media [5], pearls (interference of light inside multilayer media [15] was dealt with), and rough surfaces coated with a thin film [12].

The main purpose of the rendering methods described is to develop an efficient illumination model to render optical effects caused by specific objects such as those of a transparent nature. Each rendering algorithm is specified to render a particular kind of object. Therefore, these methods cannot

The Visual Computer (2001) 17:106–120

be used to render scenes involving different types of optical phenomena. Furthermore, in the industrial design of optical filters, half mirrors, and the like, it is necessary to accurately visualize optical properties. Illumination models proposed in various articles [10, 12, 15, 19, 20], however, do not consider multiple reflection and refraction of light inside the films. Illumination models proposed in other articles [3, 4, 8, 13] take into account multiple reflection and refraction inside a film, but cannot handle multilayered films. The illumination models proposed by Dorsey and Hanrahan [5] consider multiple reflection and refraction inside multilayer films, but cannot render the effects of interference, as their method does not consider the phase of light waves.

To accurately visualize optical phenomena caused by various kinds of objects, we need a generalized illumination model based on wave optics that can compute multiple reflections and refraction of light inside multilayer films, and can also take into account light wave phases. Furthermore, the illumination model must be able to compute, not RGB color components, but spectral distributions of light, as reflection, refraction, and interference of light inside multilayer films that greatly depend on light wavelength. The spectral distributions are subsequently converted into RGB color components for display on a color monitor, bearing human spectral tristimulus values in mind.

This paper proposes a rendering method to visualize optical properties of multilayer thin films, taking into account multiple reflection and refraction of light inside the multilayer thin films. Our method is based on wave optics described by Born and Wolf [1], and visualizes optical phenomena caused not only by dielectric multilayer films [11], but also by multilayer films consisting of metallic and/or semiconductive materials, that absorb light and have complex refractive indices. It is very important to visualize metallic and semiconductive films, since they are utilized in a wide variety of optical products such as half mirrors. The proposed method makes it possible to visualize optical properties of numerous optical products with multilayer films consisting of different kinds of materials such as dielectrics, metals, and semiconductors.

In the following section, we describe a proposed method for calculating a composite reflectance and transmittance of the system of multilayer thin films, taking into account multiple reflection and refraction, interference, and absorption of light inside the films. In Sect. 3, we implement a method using a raytracer called a multilayer film raytracer. Finally, in Sect. 4, interference colors of a SiO_2 film, and coated windowpanes or teapots with different kinds of films are visualized by the raytracer to demonstrate the usefulness of the proposed method.

2 Calculating reflectances and transmittances of multilayer films

The method proposed by Hirayama et al. [11] can calculate reflectance and transmittance of dielectric multilayer films, but cannot calculate those of metallic or semiconductive multilayer films. A great difference between dielectric and metallic materials is the absorption of light; i.e., a light passing through a metallic film is attenuated by absorption, while dielectric materials do not absorb it at all.

We have extended the method of Hirayama et al. to be able to calculate reflectances and transmittances of multilayer films consisting of materials with complex refractive indices. The method can calculate reflectance and transmittance of both dielectric and metallic multilayer films, and takes into account multiple reflection and refraction, interference, and absorption of light inside the films.

2.1 Preconditions

To visualize a light reflected on or passing through multilayer films consisting of dielectric, metallic, and/or semiconductive materials, it is necessary to calculate a composite reflectance and transmittance of the multilayer film system based on wave optics

Now we consider the system of the multilayer films that has N layers; the films are placed between two media (Fig. 1). The media extend infinitely in the opposite directions of the interfaces of the films. We assume the following preconditions for the multilayer film system.

1. Each boundary plane between the layers is smooth and parallel to the xy plane in a local coordinate system, and each layer may have a different thickness. Based on this precondition, light reflects in

the direction of mirror reflection, and transmits in the direction obeying Snell's law at the boundaries between layers.
2. The media of each layer are homogeneous and isotropic. If the index of refraction changes continuously inside a layer, the layer is further divided until it can be considered homogeneous.
3. Light comes in parallel to the zx plane from the 0th layer, and intersects the boundary plane B_1 between the L_0 and L_1 layers. As a result of multiple reflection and refraction of light inside the system of the multilayer films, the light is reflected to the 0th layer and is transmitted to the $(N+1)$th layer. A refractive index of the 0th layer should be a real value, i.e., there is no absorption in the 0th layer, since we assume the 0th layer extends infinitely. If the layer has absorption, light does not reach the boundary plane at all.

In the rendering process, incident light and films defined in world coordinates are transformed into local coordinates defined in the preconditions, and composite reflectance and transmittance of the system of the multilayer films are calculated by a recursive composition method, which is described in the next section.

2.2 Recursive composition method

We consider the system of multilayer films shown in Fig. 1. Specifying a thickness and a refractive index for each layer, we can calculate reflectivity and transmissivity of each boundary plane based on wave optics [1]. Reflectivity and transmissivity are ratios of amplitudes of incident electromagnetic waves versus reflected and transmitted electromagnetic waves, respectively. Taking into consideration phase differences between both boundaries of layers, we make a composite of the reflectivity and transmissivity in the order of the boundary planes from B_{N+1} to B_1. Finally, the composite reflectivity and transmissivity are converted into reflectance and transmittance, which represent ratios of the energies of electromagnetic waves.

Assuming that the thickness and complex refractive index of jth layer are d_j and $\widehat{n}_j$, respectively, the composite reflectivity and transmissivity between the B_{N+1} and B_{j+1} boundaries are γ_{N-j} and τ_{N-j}, respectively. The composite reflectivity γ_0 and the transmissivity τ_0 are those of the last boundary planes B_{N+1}. The seed equations at the B_{N+1} boundary plane are

$$\gamma_0 = r_{N+1}, \tag{1}$$

$$\tau_0 = t_{N+1}, \tag{2}$$

where r_{N+1} and t_{N+1} are the reflectivity and transmissivity at a single boundary B_{N+1}. After we compute the composite reflectivity γ_{N-j} and the transmissivity τ_{N-j}, the composite reflectivity and transmissivity of the next boundary plane under the condition of multiple reflection and refraction can be calculated with the following recurrence equations [1, 11] (see Appendix).

$$\gamma_{N-j+1} = \frac{r_j + \gamma_{N-j}\, e^{2i\varphi_j}}{1 + r_j\, \gamma_{N-j}\, e^{2i\varphi_j}}, \tag{3}$$

$$\tau_{N-j+1} = \frac{t_j \tau_{N-j}\, e^{i\varphi_j}}{1 + r_j\, \gamma_{N-j}\, e^{2i\varphi_j}}, \tag{4}$$

where i denotes an imaginary number, r_j and t_j are the reflectivity and transmissivity at a single boundary B_j, respectively. φ_j is the phase difference between boundary planes B_j and B_{j+1}, and is expressed by the following equation.

$$\varphi_j = \frac{2\pi}{\lambda} \widehat{n}_j d_j s_{z,j}, \tag{5}$$

where λ is the wavelength of light in a vacuum, d_j is the thickness of jth layer, $s_{z,j}$ is a z component of the unit vector $\mathbf{s}_j$ that indicates the direction of light in jth layer, and $\widehat{n}_j$ is the complex refractive index consisting of a refractive index n_j and an extinction coefficient κ_j, $(\widehat{n}_j = n_j + i\,\kappa_j)$. The unit direction vector $\mathbf{s}_j = (s_{x,j}, s_{y,j}, s_{z,j})$, is derived from Snell's law.

$$s_{x,j} = \frac{n_0 \sin\theta_0}{\widehat{n}_j}, \quad s_{y,j} = 0, \quad s_{z,j} = \sqrt{1 - s_{x,j}^2}. \tag{6}$$

Note that the unit direction vector $\mathbf{s}_j$ of each layer is derived from the refractive index n_0 the incident angle θ_0 of the 0th layer, and the complex refractive index $\widehat{n}_j$ of each layer, as we consider a system of multilayer films with boundary planes that are parallel to each other. The reflectivity r_j and the transmissivity t_j at boundary plane B_j are derived by Fresnel formulae. They are represented by a component $\parallel$ and a component $\perp$ of the electromagnetic waves that are

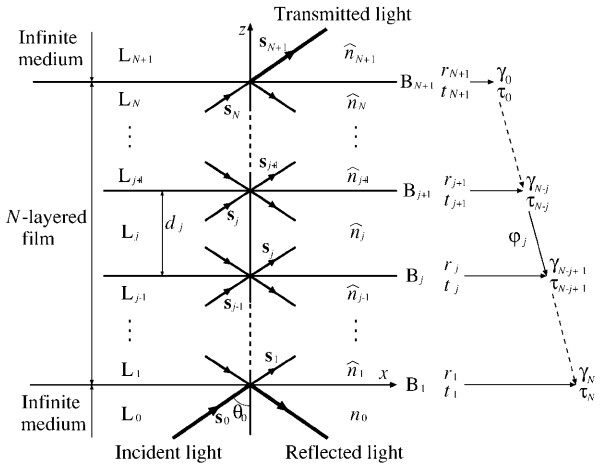

L_j : j-th layer
B_j : boundary plane between layers L_{j-1} and L_j
$\widehat{n}_j$: complex refractive index of j-th layer
n_j : refractive index of j-th layer
$\mathbf{s}_j$: unit incident direction vector of j-th layer
θ_0 : incident angle at boundary B_1
r_j : reflectivity at boundary B_j
t_j : transmissivity at boundary B_j
γ_{N-j} : composite reflectivity between j-th and $(N+1)$th boundary
τ_{N-j} : composite transmissivity between j-th and $(N+1)$th boundary
φ_j : phase difference between both boundary planes at j-th layer

Fig. 1. The system of N-layered films

parallel and perpendicular, respectively, to the incident plane of the light.

$$r_{\parallel j} = \frac{\widehat{n}_j s_{z,j-1} - \widehat{n}_{j-1} s_{z,j}}{\widehat{n}_j s_{z,j-1} + \widehat{n}_{j-1} s_{z,j}}, \tag{7}$$

$$r_{\perp j} = \frac{\widehat{n}_{j-1} s_{z,j-1} - \widehat{n}_j s_{z,j}}{\widehat{n}_{j-1} s_{z,j-1} + \widehat{n}_j s_{z,j}}, \tag{8}$$

$$t_{\parallel j} = \frac{2\widehat{n}_{j-1} s_{z,j-1}}{\widehat{n}_j s_{z,j-1} + \widehat{n}_{j-1} s_{z,j}}, \tag{9}$$

$$t_{\perp j} = \frac{2\widehat{n}_{j-1} s_{z,j-1}}{\widehat{n}_{j-1} s_{z,j-1} + \widehat{n}_j s_{z,j}}. \tag{10}$$

Equations (3) and (4) are used repeatedly to calculate each component of the composite reflectivities $\gamma_{\parallel N}$ and $\gamma_{\perp N}$ and the transmissivities $\tau_{\parallel N}$ and $\tau_{\perp N}$, of the system of the N-layer film. The reflectivities and transmissivities represent the ratios of the amplitudes of reflected and transmitted electromagnetic waves, respectively. However, the reflectance and transmittance represent the ratio of energies of reflected and transmitted electromagnetic waves, respectively. To convert the amplitudes into energy, we take a square of the absolute value of the coefficients. We calculate a composite reflectance $\mathcal{R}$ and transmittance $\mathcal{T}$ of the system of the multilayer films by averaging the energies of the parallel and perpendicular components because the contributions of these two components to the reflectance and transmittance are usually equal.

$$\mathcal{R} = \frac{\left|\gamma_{\parallel N}\right|^2 + \left|\gamma_{\perp N}\right|^2}{2}, \tag{11}$$

$$\mathcal{T} = \begin{cases} \dfrac{\widehat{n}_{N+1}\, s_{z,N+1}}{n_0\, s_{z,0}} \dfrac{\left|\tau_{\parallel N}\right|^2 + \left|\tau_{\perp N}\right|^2}{2} \\ \qquad (\widehat{n}_{N+1} \text{ is a real number}), \\ 0 \qquad (\widehat{n}_{N+1} \text{ is a complex number}). \end{cases} \tag{12}$$

Note that the transmittance becomes zero when $\widehat{n}_{N+1}$ is a complex number because the $(N+1)$th layer has the capacity of light absorption. Consequently, the method for obtaining the composite reflectance and transmittance of the system of the multilayer films is as follows.

1. Given a complex refractive index $\widehat{n}_j$ and a thickness d_j of each layer, then the phase change φ_j, reflectivities $r_{\parallel j}$ and $r_{\perp j}$, and the transmissivities $t_{\parallel j}$ and $t_{\perp j}$ are calculated for an incident light intersecting the multilayer films with angle θ_0. Equation (5) and (7)–(10) are used for this purpose.
2. We calculate the composite reflectivities $\gamma_{\parallel j}$ and $\gamma_{\perp j}$ and the composite transmissivities $\tau_{\parallel j}$ and $\tau_{\perp j}$ by repeatedly using (3) and (4), respectively. (1) and (2) are the seed equations for (3) and (4), respectively.

3. We calculate a composite reflectance $\mathcal{R}$ and a composite transmittance $\mathcal{T}$ of the system of the multilayer films with (11) and (12), respectively.

2.3 Discussion of multiple reflection and refraction

In this section, we discuss how important the consideration of multiple reflections and refractions inside films is for calculating composite reflectances and transmittances. Figure 2 shows the simulation results of reflectances and transmittances under the conditions of limited numbers of multiple reflections and refractions. We calculate these reflectances and transmittances with (11), (12), (14), and (15), changing the number of reflections and refractions m (see Fig. 11). In the simulation, the dielectric medium with a refractive index of 2.0 is coated with a 10 nm gold film.

As shown in the simulation results (Fig. 2), the number of multiple reflections and refractions of light plays an important role in the accurate calculation of reflectances and transmittances. Even in the case of the fifth reflection and refraction, an approximation error remains. To make matters worse, when the number of reflections and refractions is small (e.g., $m = 0, 1$), the transmittance exceeds 1.0. The larger the reflectance of multilayer films, the more carefully the number of multiple reflections and refractions should be taken into account. With the proposed method, we can calculated the reflectances and transmittances of a multilayer film system, taking into account the infinite number of multiple reflections and refractions at all the boundaries of the system.

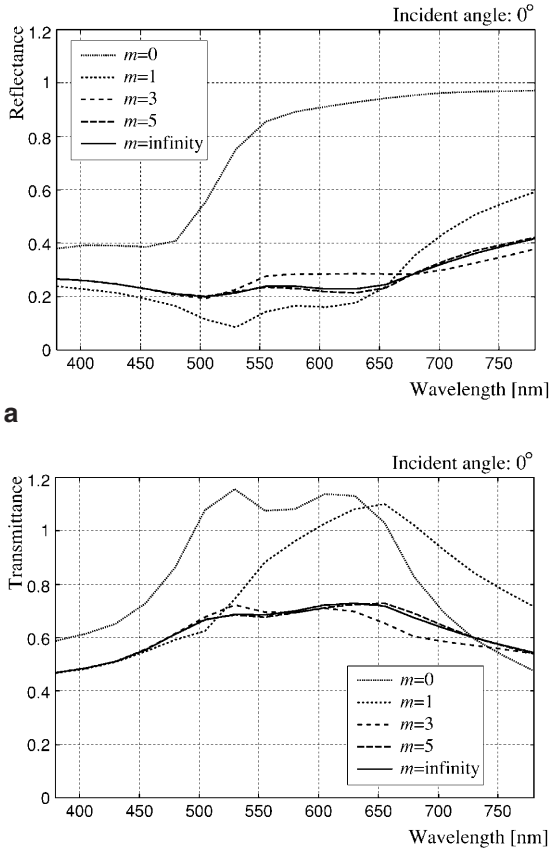

Fig. 2a,b. Simulation results of reflectances and transmittances: **a** reflectance of a film; **b** transmittance of a film. [L_0, air, L_1, 10 nm gold; L_2, dielectric ($n = 2.0$)]

3 Implementation of the multilayer film raytracer

We extend the raytracer proposed by Hirayama et al. [11] to visualize both dielectric multilayers and multilayers with absorption of light such as those with metallic or semiconductive films. In this section, we discuss the implementation of the multilayer film raytracer.

Figure 3 shows an algorithm of our raytracer. The raytracer calculates a composite reflectance and transmittance for each wavelength of light prior to the raytracing process. In the raytracing process, a spectral distribution of light is calculated for each ray. Finally, spectral distributions of light rays are converted into RGB values to display a generated image on a monitor.

3.1 Calculation of composite reflectances and transmittances

Reflection and transmission properties of multilayer films are determined by refractive indices and thicknesses consisting of the system of the multilayer films. In the modeling process, refractive indices and thicknesses of each film are specified as surface attributes of objects. In the rendering preprocess, composite reflectances and transmittances of

the system of multilayer films are calculated by the proposed method, described in Sect. 2, for each sampled incident angle and wavelength of light. This information is then stored in tables. Note that these tables are two dimensional, as the reflectance and transmittance depend on both an incident angle and a wavelength of light. Furthermore, two tables are required when (1) each side of a multilayer film faces different kinds of media, and (2) light rays come from both sides of the films, as the composite reflectances and transmittances are different according to the interface with which a light ray first intersects.

If the size of all the tables exceeds the memory capacity of a computer, these tables can be compressed with an advanced compression algorithm, such as a wavelet composition.

3.2 Raytracing process

In the raytracing process (Fig. 4), each object is first checked to see whether a ray intersects with it. To accelerate the intersection test, bounding boxes of objects, including free-form surfaces, are employed. If a ray intersects a transparent object or a surface with specular reflection, then the reflectance and transmittance at the intersection point are linearly interpolated from the precalculated tables. In this case, the ray produces reflected and transmitted rays, which are then traced recursively. Only a single ray is used to trace reflected or transmitted light for all wavelengths of light because the films are very thin. The intensities of the reflected and transmitted rays are multiplied by the composite reflectance and transmittance. Note that this process is carried out even when the ray intersects a surface without a film. We can also calculate the reflectance and the transmittance of a film-free surface by setting the number of layers to zero and, using the recursive composition method described in Sect. 2.2.

If the ray intersects a perfectly diffuse surface, the intensities of diffuse light for each wavelength are calculated. If the ray does not intersect any object, the intensities of a background are set.

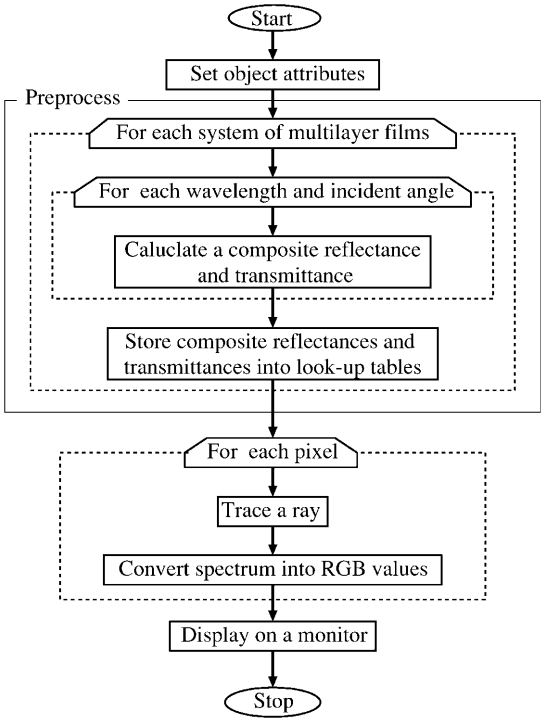

3

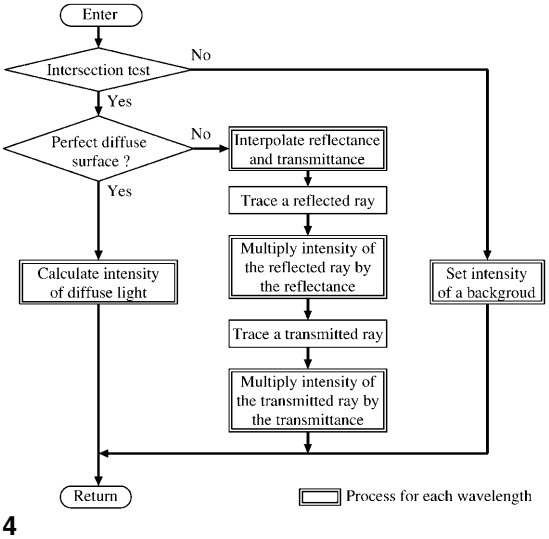

4

Fig. 3. Algorithm of the multilayer film raytracer

Fig. 4. Raytracing process

3.3 Rendering free-form surfaces

To calculate intersections of a ray with free-form surfaces, a Bézier clipping [16] is implemented to our multilayer film raytracer. The Bézier clipping quickly calculates intersections of a ray with Bézier surfaces by clipping the surfaces recursively until the clipped area can be considered a point. However, the method has a problem with triangular patches: it

fails to calculate intersections near the degenerated vertex of a triangular Bézier patch (for example, the top of the handle of a Utah teapot). This is because the surface is clipped repeatedly in (u, v) parameter space. The method does not converge, as the clipped area does not become smaller in (u, v) parameter space, while it converges enough in (x, y, z) coordinate space. To solve the problem, every time a triangular Bézier patch is clipped, the clipped region of a u or v direction with a degenerated vertex is converted into (x, y, z) coordinate space, and the convergence is judged in (x, y, z) coordinate space.

3.4 Color representation by spectral distributions

Conventional raytracers calculate the intensities of RGB colors corresponding to red, green, and blue monochromatic light. However, it is necessary to calculate the spectrum of light to accurately render optical phenomena. Particularly in reflection, refraction, interference, and absorption of light inside films, the optical characteristics greatly depend on a light wavelength. For this reason, our multilayer film raytracer calculates a spectrum distribution of light.

There are several methods for sampling a wavelength of light. An adaptive sampling is a good method for a lighting model in an interference-free environment because we only take into account spectrum of light. In the interference environment, however, many factors should be considered in the sampling of the light wavelength, including spectrum of light, incident angles of light rays, and the reflectivities and transmissivities of boundaries of each layer. In the raytracer, a constant sampling is employed, i.e., the wavelength of visible light (380 nm to 780 nm) is sampled every 5 nm.

After calculating reflected and transmitted light from multilayer films, the light spectra are converted into RGB values to display on a color monitor with the spectral tristimulus values of the RGB colorimetric system [6].

$$R = \sum_{\lambda} r_{\lambda} I_{\lambda}, \quad G = \sum_{\lambda} g_{\lambda} I_{\lambda}, \quad B = \sum_{\lambda} b_{\lambda} I_{\lambda}, \tag{13}$$

where λ is a sampled wavelength, r_{λ}, g_{λ}, and b_{λ} are the spectral tristimulus values, and I_{λ} is a spectrum of light for each sampled wavelength.

4 Examples

Interference colors caused by a SiO_2 layer on a silicon base and a scene containing windowpanes coated with multilayer films were rendered to show the usefulness of the proposed method. The refractive indices used in these examples were obtained by Palik [18].

4.1 Interference color of a SiO_2 layer on a silicon base

Figure 5a shows interference colors caused by a SiO_2 layer on a silicon base, and we calculated it with the proposed method by sampling the wavelength of visible light every 5 nm. The horizontal and vertical axes in Fig. 5 correspond to the incident angle of the viewing ray and the thickness of a SiO_2 layer, respectively. The spectral distribution of a light source is set to the CIE standard illuminant D_{65} [7]. Figure 5b shows interference colors calculated by sampling the RGB colors corresponding to red (700 nm), green (545 nm), and blue (435 nm) monochromatic light. The color calculated by the proposed method is accurately simulated in the region where the incident angle of light is nearly 90° (the reflectance of the SiO_2 layer in this region is almost 1). Furthermore, when we compare the interference colors in these figures, we see that the thicker the SiO_2 layer, the more the interference color differs. Figure 5c shows the color differences between Fig. 5a and b, and the intensities of each pixel are multiplied by 3 to clearly visualize the differences. The maximal color differences between Fig. 5a and b for the R, G, and B color components are 47, 33, and 43, respectively, in 256 intensity levels.

We also compared the interference colors in Fig. 5a with those of seven samples of silicon bases coated with SiO_2 layers of different thicknesses (Fig. 6). If we observe the samples from different viewing directions, we see that the interference colors we visualized are almost the same as those of the samples.

4.2 Simulation of windowpanes coated with multilayer films

Building windowpanes coated with multilayer films are rendered by our multilayer film raytracer. Reflection and transmission properties of windowpanes

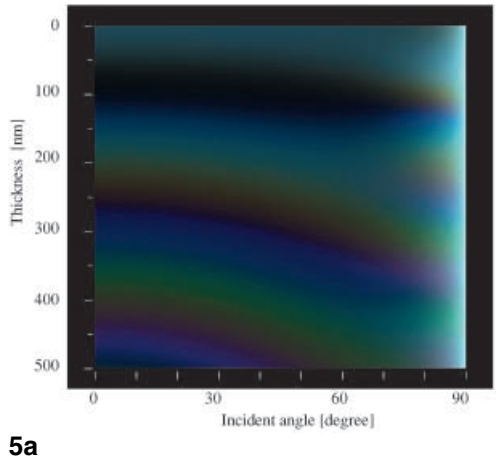

5a

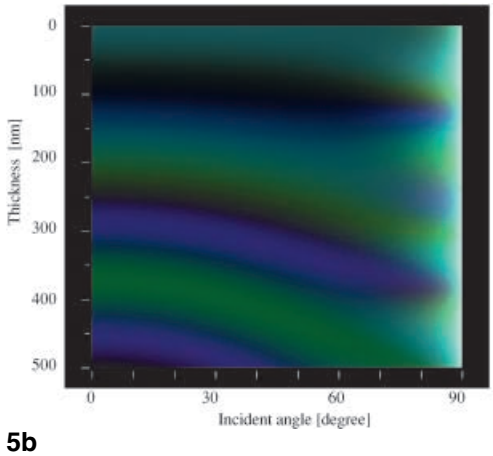

5b

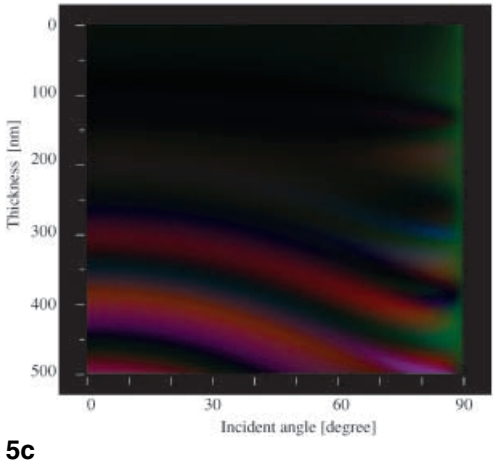

5c

6

Fig. 5a–c. Interference colors caused by a SiO_2 layer: **a** proposed method; **b** sampled RGB wavelengths; **c** color differences
Fig. 6. Samples of silicon bases coated with a SiO_2 layer of different thicknesses

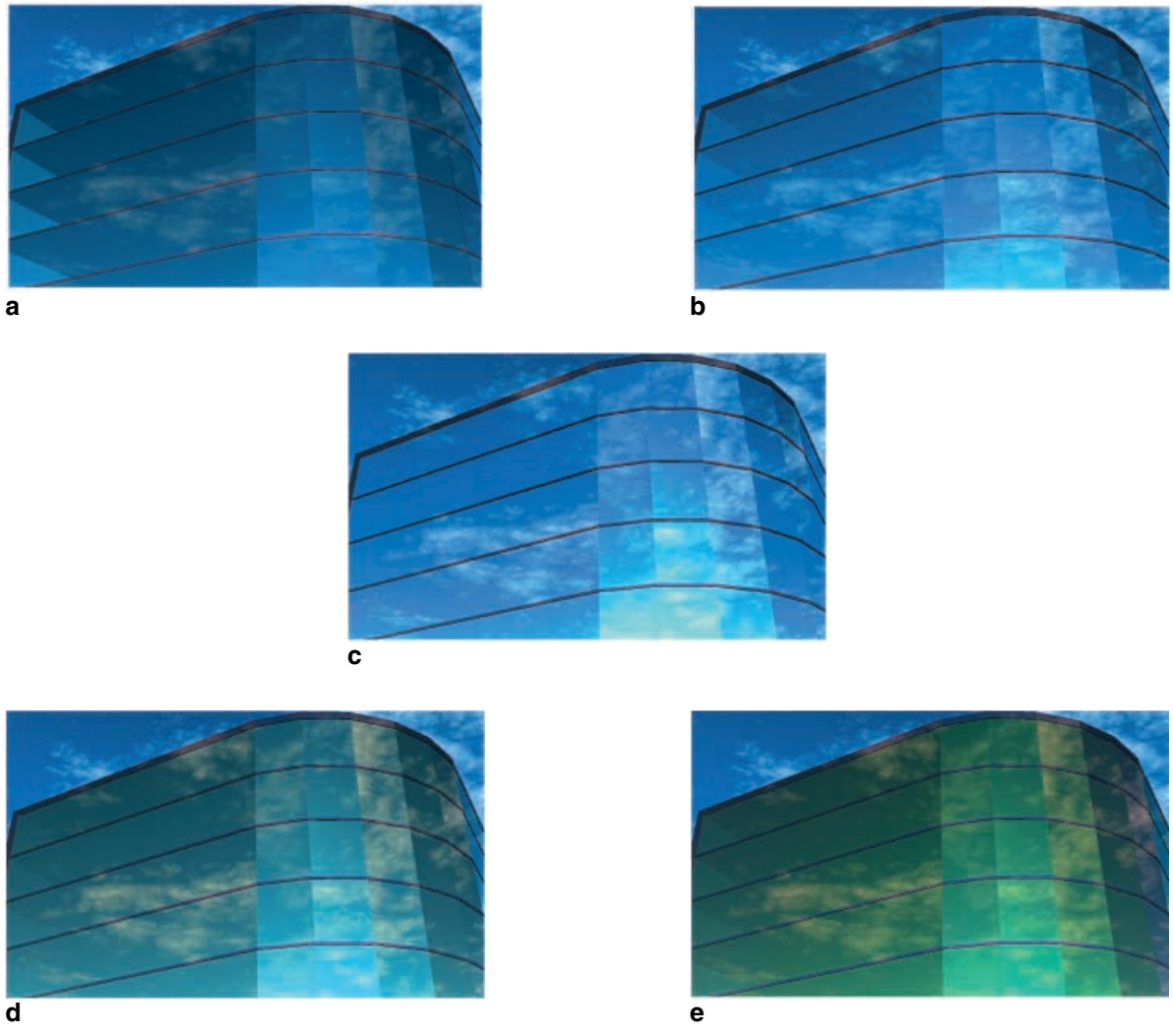

Fig. 7a–e. Windowpanes coated with various films: **a** aluminum film (5 nm); **b** aluminum film (10 nm); **c** aluminum film (20 nm); **d** multilayer metallic films; **e** dielectric and metallic films

coated with dielectric and metallic films are evaluated visually with the proposed method.

Images of windowpanes rendered by the multilayer film raytracer are shown in Fig. 7, and several graphs of reflectance distributions for incident angles and wavelength of light are shown in Fig. 8. Refractive indices of glass and a dielectric material used in Fig. 7 are set to 1.6 and 2.0, respectively, for all visible wavelengths of light, and these materials do not absorb any light. Films are coated on the outside surfaces of the windowpanes, and the film materials and their thicknesses are shown in Table 1. Refractive indices of metallic materials, such as aluminum and gold, greatly depend on the wavelength of light, and were obtained by Palik [18]. The spectral distribution of the sky color was calculated with an atmospheric scattering model [17], and the spectral distribution of clouds was considered as white light with an equal-energy spectrum.

Figure 7a–c shows views of windowpanes coated with aluminum films of various thicknesses. Comparing the panels of the figure, the thicker the aluminum films, the more the sky is reflected in the

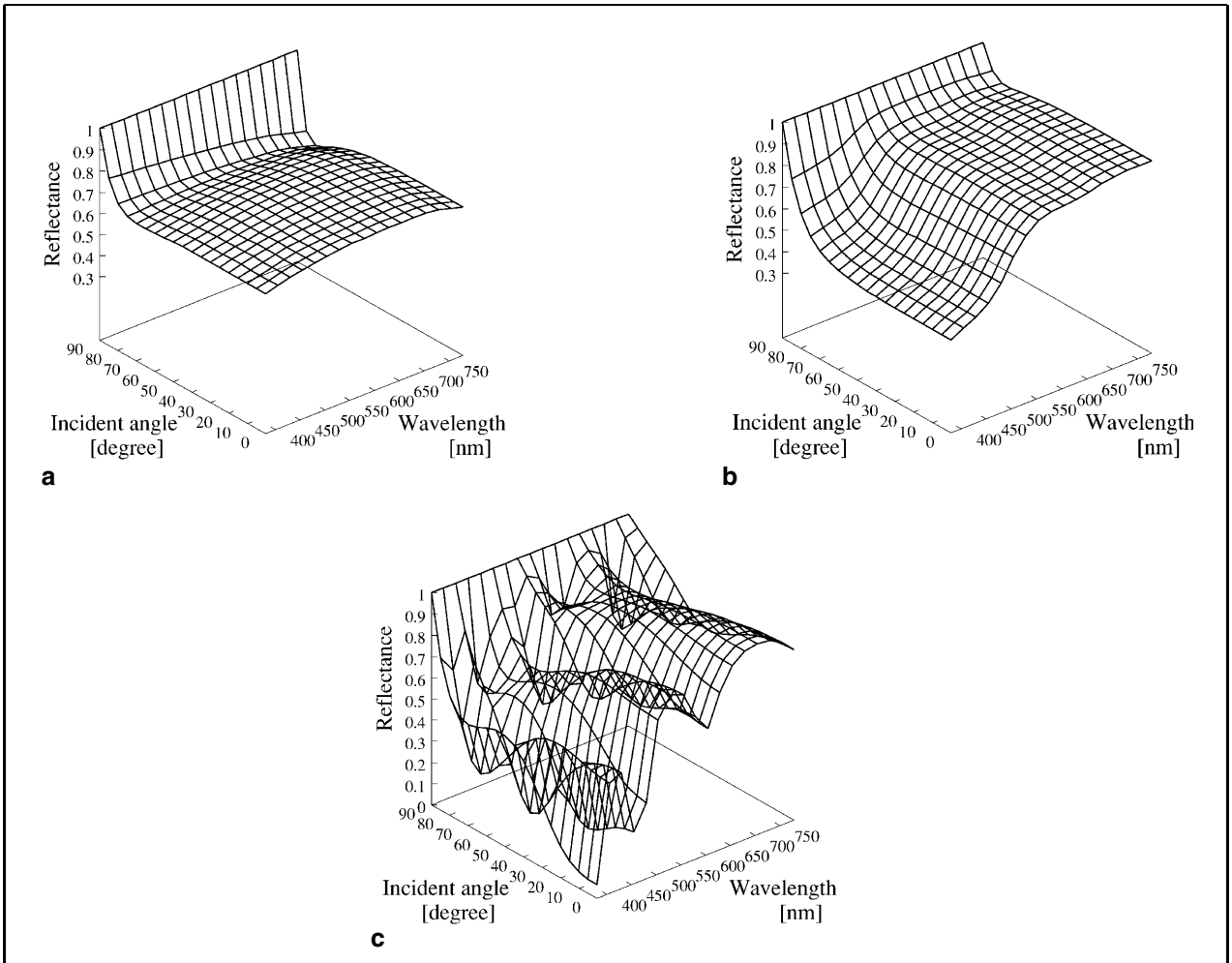

Fig. 8a–c. Graphs of reflectance distributions – windowpanes in: **a** Fig. 7b; **b** Fig. 7d; **c** Fig. 7e

windowpanes. In Fig. 7c, the inside of the building is hardly seen through the windowpanes, while the inside can be seen in Fig. 7a. This is because the thicker the film, the larger the reflectance of the windowpanes coated with an aluminum film becomes. The absorption of light inside the aluminum films also increases, and the transmittance of the windowpanes becomes smaller.

Figure 7d shows windowpanes coated with multilayer films consisting of gold and aluminum. The blue sky is not reflected much in the windowpanes, while clouds are reflected clearly. This is because the reflectance of light with a short wavelength is lower than that with a long wavelength (Fig. 8b). Figure 7e shows windowpanes coated with both dielectric and metallic films. The color of clouds reflected in the windowpanes are yellow or purple, because of the interference inside the dielectric films. The reflectance distribution of the windowpanes in Fig. 7e is shown in Fig. 8c.

The size of the rendered images in Fig. 7 is 1000×600 pixels, and it took 5 min to render each image on an Alpha CPU (633 MHz) workstation, including the computation time for the preprocess of rendering.

These figures visualize the properties of reflectance and transmittance of windowpanes coated with various kinds of films, and provide easy understanding of the optical properties of multilayer films.

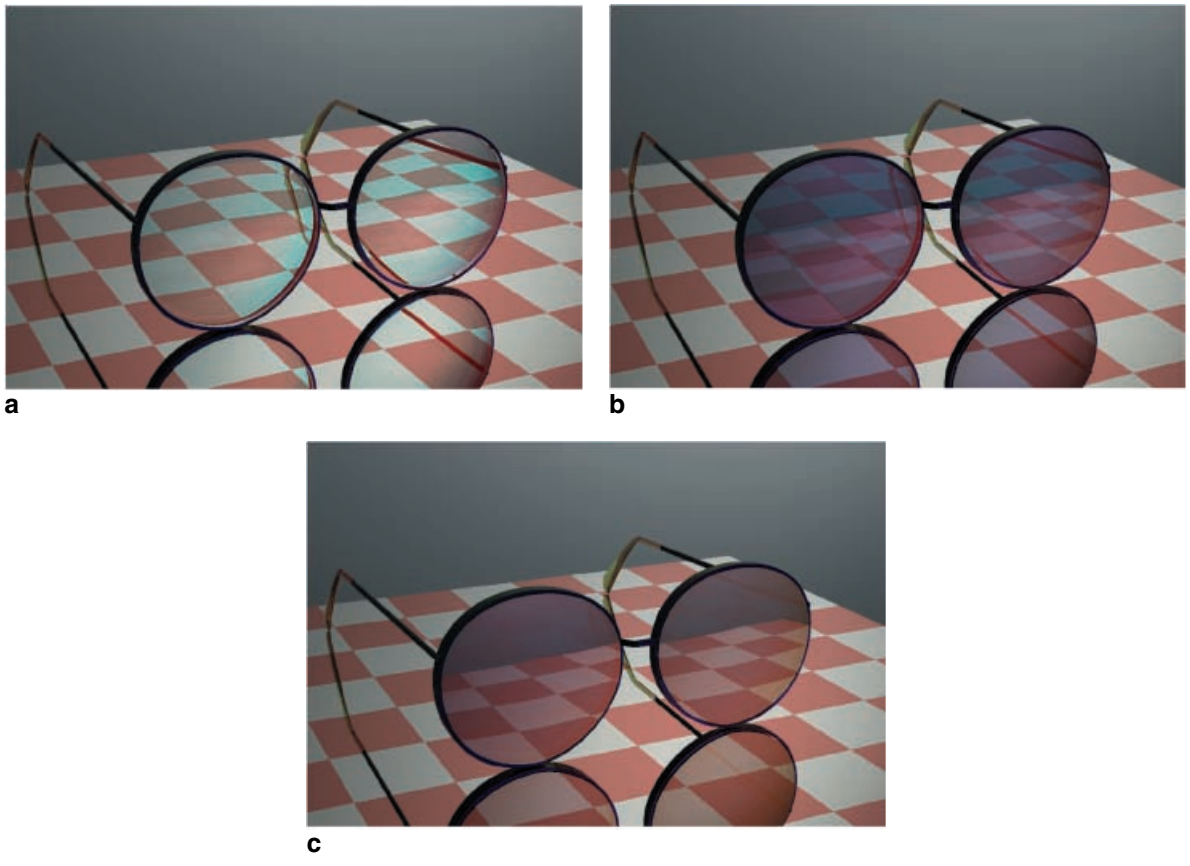

Fig. 9a–c. Glasses coated with: **a** dielectric multilayer films; **b** 300 nm dielectric and 5 nm aluminum films; **c** 300 nm dielectric and 10 nm aluminum films

4.3 Glasses and teapots coated with films

To show the usefulness of our raytracer for designing various kinds of industrial products having free-form surfaces, several images of glasses and teapots modeled with Bézier surfaces were rendered.

In Fig. 9a, glasses are coated with six-layered films consisting of two kinds of 100 nm dielectric films with refractive indices of 2.0 and 1.6 alternately, while, in Fig. 9b and c, glasses are coated with multilayer films consisting of a dielectric with a refractive index of 2.0 and an aluminum film. Lenses of the glasses are modeled with 24 Bézier patches, and are made of dielectric media with refractive indices of 1.6. A point light source with the sepectral distribution of the CIE standard illuminant D_{65} [7] is set above the glasses. With dielectric multilayer films, light is almost transmitted through the lenses (Fig. 9a), while the checkered plate reflected into the lenses with a metallic film can be observed in Fig. 9b, and the lenses look bluish because of light absorption due to an aluminum layer. The thicker the aluminum film, the less the light is transmitted through the lenses, and light is almost reflected on the lenses as shown in Fig. 9c.

Figure 10a shows a teapot made of silicon coated with a 500 nm SiO_2 film. Figure 10b shows a glass teapot coated with a 20 nm gold film, while Fig. 10c shows a glass teapot coated with 10 nm aluminum, 20 nm gold, and 500 nm dielectric films. A checkered plate under the teapot is made of silver and copper, except in Fig. 10d. A point light source with the sepectral distribution of the CIE standard illuminant D_{65} [7] is set above the teapot.

Color changes of interference inside a SiO_2 film appear on the surface of the teapot in Fig. 10a. In

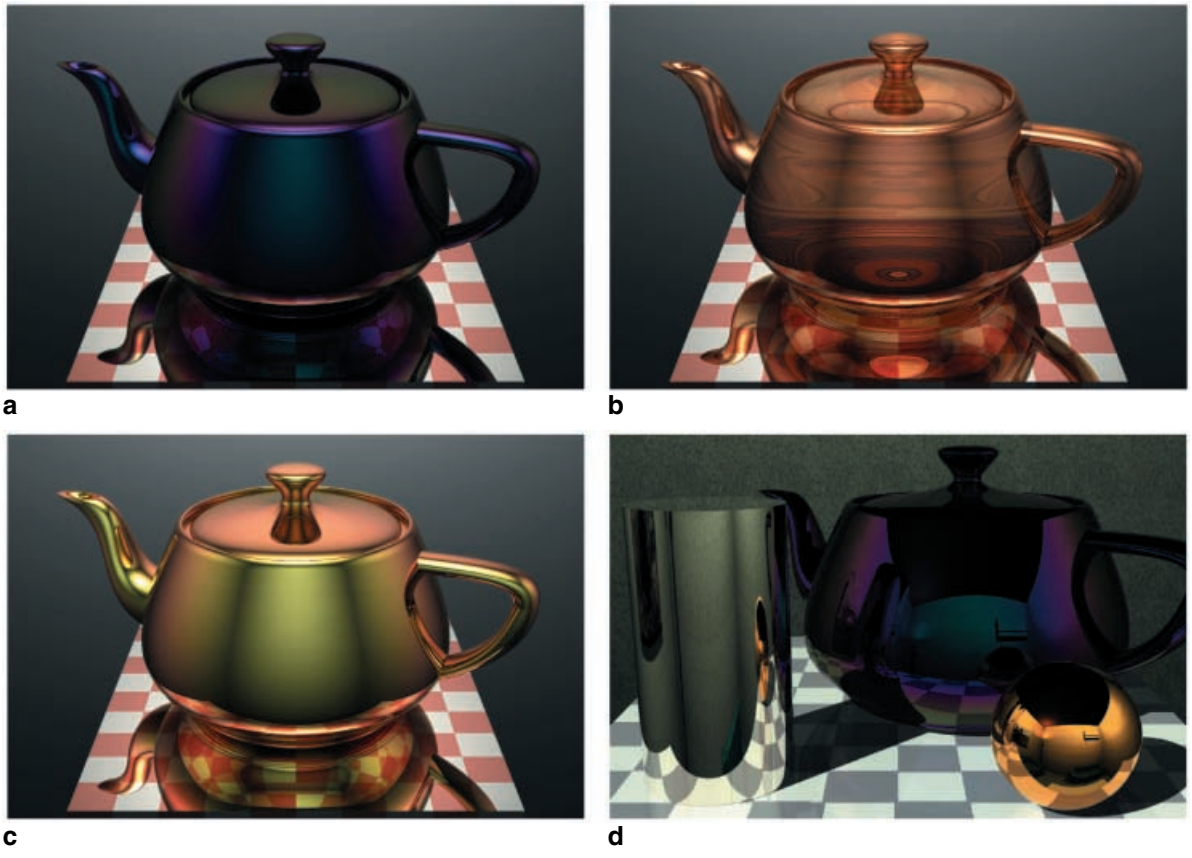

Fig. 10a–d. Silicon teapot coated with a SiO_2 film; **b** glass teapot with gold film; **c** glass teapot with aluminum, gold and dielectric films; **d** silicon teapot with SiO_2 film, copper cylinder with a gold film, and copper sphere with a silver film

Fig. 10b, absorption of light occurs inside a gold film due to the complex refraction index of gold, but some light is transmitted by the teapot because the gold film is very thin. In Fig. 10c, both interference and absorption of light are observed, and the surface of the teapot is reddish due to interference of light inside the dielectric film.

In Fig. 10d, a silicon teapot, a copper cylinder, and a copper sphere are coated with a 500 nm SiO_2 film, a 50 nm silver film, and a 50 nm gold film, respectively. The checkered plate under the teapot is a diffuse surface. To visualize the effects of the thickness of each film, two kinds of animations are generated, so that the thickness of each film changes from 1 nm to 50 nm for the silver and gold films, and from 1 nm to 500 nm for the SiO_2 film (see http://www.eml.hiroshima-u.ac.jp/gallery/Animation/film/index.html).

5 Conclusions

In this paper, we have proposed a method for rendering objects coated with multilayer films consisting of dielectric, metallic and/or semiconductive materials, taking into consideration complex refractive indices. We implemented the proposed method in a raytracer called the multilayer film raytracer, and rendered objects coated with different kinds of multilayer thin films to show the usefulness of the method. The proposed method makes it possible to visualize accurate reflectance and transmittance properties of objects coated with multilayer films.

The proposed method can handle only ideal smooth surfaces coated with multilayer films. One of the future studies is developing a method for handling rough surfaces coated with multilayer films.

Acknowledgements. The authors thank Dr. Seiichi Miyazaki and Dr. Atsushi Kohno for their discussions and for providing the samples of a SiO_2 layer.

References

1. Born M, Wolf E (1997) Principles of optics. Cambridge University Press, United Kingdom
2. Cook RL, Torrance KE (1982) A reflectance model for computer graphics. ACM Trans Graph 1:7–24
3. Dias ML (1991) Ray tracing interference color. IEEE Comput Graph Appl 11:54–60
4. Dias ML (1994) Ray tracing interference color: visualizing newton's rings. IEEE Comput Graph Appl 14:17–20
5. Dorsey J, Hanrahan P (1996) Modeling and rendering of metallic paints. Proc. SIGGRAPH '96 Annual Conference Series on Computer Graphics, ACM SIGGRAPH, pp 387–396
6. Glassner AS (1995a) Principles of digital image synthesis 1. Morgan Kaufmann, San Francisco, Calif, pp 44–51
7. Glassner AS (1995b) Principles of digital image synthesis 2. Morgan Kaufmann, San Francisco, Calif, pp 1172–1175
8. Gondek JS, Meyer GW, Newman JG (1994) Wavelength dependent reflectance functions. Proc. SIGGRAPH '94 Annual Conference Series on Computer Graphics, ACM SIGGRAPH, pp 213–220
9. Hall RA, Greenberg DP (1983) A testbed for realistic image synthesis. IEEE Comput Graph Appl 3:10–20
10. Hanrahan P, Wolfgang K (1993) Reflection from layerd surfaces due to subsurfaces scattering. Proc. SIGGRAPH '93 Annual Conference Series on Computer Graphics, ACM SIGGRAPH, pp 165–174
11. Hirayama H, Monden Y, Kaneda K, Yamashita H (1998) Scientific visualization of wave scattering phenomena of transparent optical systems. (in Japanese) J Institute Image Electronics Eng Japan 27:306–317
12. Icart I, Arques D (1999) An illumination model for a system of isotropic substrate-isotropic thin film with identical rough boundaries. Proceedings of the 10th Eurographics Workshop on Rendering, Granada, Spain, pp 261–272
13. Li J, Peng Q (1996) A new illumination model for scenes containing thin film interference. Chinese J Electronics 5:18–24
14. Moravec, HP (1981) 3D graphics and the wave theory. (SIGGRAPH '81) Comput Graph 15:289–296
15. Nagata N, Dobashi T, Manabe Y, Usami T, Inokuchi S (1997) Modeling and visualization for a pearl-quality evaluation simulator. IEEE Trans Vis Comput Graph 3:307–315
16. Nishita T, Sederberg TW, Kakimoto M (1990) Ray tracing trimmed rational surface patches. (SIGGRAPH '90) Comput Graph 24(4):337–345
17. Nishita T, Sirai T, Tadamura K, Nakamae E (1993) Display of the earth taking into account atmospheric scattering. (SIGGRAPH '93) Annual Conference Series on Computer Graphics, ACM SIGGRAPH, pp 175–182
18. Palik ED (1985) Handbook of optical constants of solids. Academic Press, Orlando
19. Smits BE, Meyer GW (1990) Newton's colors: Simulating interference phenomena in realistic image synthesis. Proceedings of Eurographics Workshop on Photosimulation, Realism and Physics. Comput Graph pp 185–194
20. Suzuki N, Yokoi S, Toriwaki J (1993) Study on color computation in computer graphics and it's application to rendering color caused by light interference. (in Japanese) IEICE Technical Report of Japan 88:41–48
21. Thomas SW (1986) Dispersive refraction in ray tracing. Visual Comput 2:3–8
22. Yasuda T, Yokoi S, Toriwaki J, Tsuruoka S, Miyake Y (1984) An improved ray tracing algorithm for rendering transparent objects. (in Japanese) Trans Inform Process Soc Japan 25:953–959
23. Yokoi S, Kurashige K, Toriwaki J (1986) Rendering gems with asterism or chatoyancy. Visual Comput 2:307–312

Appendix.

Recurrence equations of composite reflectivity and transmissivity

Let us consider a three-layer film system consisting of dielectric or metallic films (Fig. 11). The generalized recurrence equations of the film system can be derived from complex refractive indicies. In the case of a dielectric film, the recurrence equations are obtained by simply replacing the complex number with a real number.

In Fig. 11, light comes from layer L_0, and is transmitted to layer L_2 with multiple reflection and refraction inside layer L_1. Assuming that the forward reflectivity and transmissivity at boundary B_1 are r_1 and t_1, respectively, and the backward reflectivity and transmissivity, i.e., those which light travels from layer L_1 to layer L_0 are r_1' and t_1', respectively, then the composite reflectivity γ and transmissivity τ of the three-layer system are expressed as follows:

$$\gamma = r_1 + \sum_{m=1}^{\infty} r_2 t_1 t_1' e^{2i\varphi_1} \left(r_1' r_2 e^{2i\varphi_1} \right)^{m-1}, \tag{14}$$

$$\tau = \sum_{m=0}^{\infty} t_1 t_2 e^{i\varphi_1} \left(r_1' r_2 e^{2i\varphi_1} \right)^{m}, \tag{15}$$

where φ_1 is the phase difference between the boundaries of layer L_1,

$$\varphi_1 = \frac{2\pi}{\lambda} \hat{n}_1 d_1 s_{z,1}, \tag{16}$$

where λ is the wavelength of light in a vacuum, and $\hat{n}_1$ is the complex refractive index, d_1 is the thickness, and $s_{z,1}$ is a z component of the unit vector $\mathbf{s}_1$ that indicates the direction of light in layer L_1. Note that (14) and (15) are infinite geometric series be-

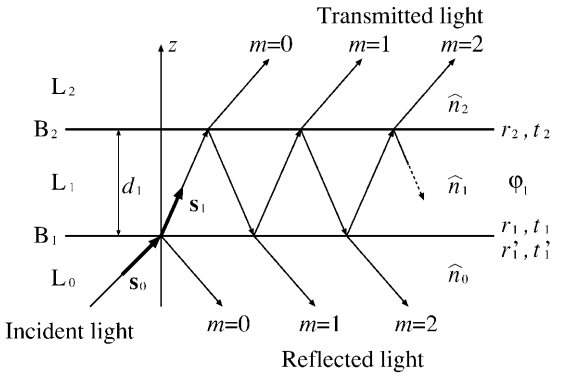

Fig. 11. The three-layer film system

cause of the multiple reflection and refraction of light between the boundaries of layer L_1.

Using the relationships between the forward and backward reflectivities/transmissivities,

$$\gamma = \lim_{m\to\infty} \frac{r_1 + \left(r_1^2 + \frac{\widehat{n}_1 s_{z,1}}{\widehat{n}_0 s_{z,0}} t_1^2\right) r_2\, e^{2i\varphi_1}}{1 + r_1 r_2\, e^{2i\varphi_1}} - \frac{r_2 \frac{\widehat{n}_1 s_{z,1}}{\widehat{n}_0 s_{z,0}} t_1^2\, e^{2i\varphi_1} \left(-r_1 r_2\, e^{2i\varphi_1}\right)^m}{1 + r_1 r_2\, e^{2i\varphi_1}}, \quad (17)$$

$$\tau = \lim_{m\to\infty} \frac{t_1 t_2\, e^{i\varphi_1} - t_1 t_2\, e^{i\varphi_1} \left(-r_1 r_2\, e^{2i\varphi_1}\right)^m}{1 + r_1 r_2\, e^{2i\varphi_1}}. \quad (18)$$

From Fresnel formulae (7)–(10), the following equation is derived.

$$r^2 + \frac{\widehat{n}_1 s_{z,1}}{\widehat{n}_0 s_{z,0}} t^2 = 1. \quad (19)$$

(17) and (18) converge as the absolute value of the common ratio of the geometric series satisfies the relation $\left|r_1 r_2 e^{2i\varphi_1}\right| < 1$. Finally, the composite reflectivity and transmissivity of the three-layer film system are derived as follows:

$$\gamma = \frac{r_1 + r_2\, e^{2i\varphi_1}}{1 + r_1 r_2\, e^{2i\varphi_1}}, \quad (20)$$

$$\tau = \frac{t_1 t_2\, e^{i\varphi_1}}{1 + r_1 r_2\, e^{2i\varphi_1}}. \quad (21)$$

When the layer L_1 is a metallic or semiconductive medium, the following coefficients are set to complex numbers:

$$\widehat{n}_1 s_{z,1} = u_1 + iv_1, \quad (22)$$

$$r_1 = \varrho_1 e^{i\delta_1}, \quad (23)$$

$$r_2 = \varrho_2 e^{i\delta_2}, \quad (24)$$

$$t_1 = \tau_1 e^{i\chi_1}, \quad (25)$$

$$t_2 = \tau_2 e^{i\chi_2}, \quad (26)$$

$$\varphi_1 = \eta_1(u_1 + iv_1), \qquad \eta_1 = \frac{2\pi}{\lambda} d_1. \quad (27)$$

Substituting (20) with (22)–(24) and (27), composite reflectivity is derived as follows:

$$\gamma = \frac{\varrho_1 e^{i\delta_1} + \varrho_2 e^{i\delta_2} e^{2i\eta_1(u_1+iv_1)}}{1 + \varrho_1 e^{i\delta_1} \varrho_2 e^{i\delta_1} e^{2i\eta_1(u_1+iv_1)}} \quad (28)$$

$$= \frac{\varrho_1 e^{i\delta_1} + \varrho_2 e^{-2v_1\eta_1} e^{i(\delta_2+2u_1\eta_1)}}{1 + \varrho_1\varrho_2 e^{-2v_1\eta_1} e^{i(\delta_1+\delta_2+2u_1\eta_1)}}. \quad (29)$$

(29) is exactly the same equation as that of Born and Wolf [1] ((20) in Sect. 13.4.1). In the same way, we can derive transmissivities when layer L_1 is a metallic or semiconductive medium. Furthermore, composite reflectivities and transmissivities for any kind of system can be derived from (20) and (21).

Repeating this process in order of layers from the transmitted light to the incident light, i.e., the inverse direction of transmission of light, the recurrence equations [(3) and (4)] are obtained.

$$\gamma_{N-j+1} = \frac{r_j + \gamma_{N-j}\, e^{2i\varphi_j}}{1 + r_j\, \gamma_{N-j}\, e^{2i\varphi_j}}, \quad (30)$$

$$\tau_{N-j+1} = \frac{t_j \tau_{N-j}\, e^{i\varphi_j}}{1 + r_j\, \gamma_{N-j}\, e^{2i\varphi_j}}. \quad (31)$$

Photographs of the authors and their biographies are given on the next page.

HIDEKI HIRAYAMA is currently a PhD candidate at the Graduate School of Engineering, Hiroshima University, Hiroshima Japan. He received his BSc and MSc in Computer Science from Shimane University, Japan, in 1996 and 1998, respectively. His research interests include scientific visualization of physical phenomena and animation of human motions. He is a member of the Information Processing Society of Japan and the Institute of Electronics, Information and Communication Engineers.

KAZUFUMI KANEDA is an Associate Professor in the Faculty of Engineering at Hiroshima University. He worked at Chugoku Electric Power, Japan, from 1984 to 1986. He joined Hiroshima University in 1986. He was a Visiting Researcher in Engineering Computer Graphics Laboratory at Brigham Young University in 1991. He received his BE, ME, and DE in 1982, 1984, and 1991, respectively, from Hiroshima University. His research interests include computer graphics, scientific visualization, and image processing. He is a member of the ACM, the IPSJ, the IEICE, and the IEEJ.

HIDEO YAMASHITA has been a Professor at the Department of Electrical Engineering, Hiroshima University, Hiroshima, Japan since 1992. He received his BE and ME in Electrical Engineering from Hiroshima University, in 1964 and 1968, respectively, and a PhD in Electrical Engineering from Waseda University, Tokyo, Japan, in 1977. His interests include electric and magnetic fields, analysis of electric machinery by finite element analysis, and visualization of 3D magnetic fields by computer graphics. He is a member of the Institute of Electrical Engineering of Japan and the IEEE.

YOSHIKI YAMAJI is currently a graduate student at the Graduate School of Engineering, Hiroshima University, Japan. He received his BE in Electrical Engineering from Hiroshima University, Hiroshima, Japan, in 1998. His research interests include modeling and visualization. He is a member of Information Processing Society of Japan.

YOSHIMI MONDEN was born in Hiroshima, Japan, in 1943 and is now with the Faculty of Science and Engineering, Shimane University. His current research interests are in algebraic algorithms of system theory, discrete modeling of physical systems, and scientific visualization of physical phenomena. Dr. Monden is a member of the Institute of Electronics, Information and Communication Engineering of Japan, the Information Processing Society of Japan, the Institute of Image Electronics Engineers of Japan, the IEEE, and the ACM.